ORNL/TM-2022/2784

Optical Simulations for the VENUS Neutron Imaging Instrument

Matthew J. Frost
Christoph U. Wildgruber
Hassina Bilheux
Kyle Grammer

November 2022

OAK RIDGE National Laboratory

ORNL IS MANAGED BY UT-BATTELLE LLC FOR THE US DEPARTMENT OF ENERGY

ORNL/TM-2022/2784

Neutron Technologies Division, Neutron Sciences Directorate

Optical Simulations for the VENUS Neutron Imaging Instrument

Matthew J. Frost
Christoph U. Wildgruber
Hassina Bilheux
Kyle Grammer

November 2022

Prepared by
OAK RIDGE NATIONAL LABORATORY
Oak Ridge, TN 37831-6283
managed by
UT-Battelle LLC
for the
US DEPARTMENT OF ENERGY
under contract DE-AC05-00OR22725

CONTENTS

LIST OF FIGURES

LIST OF TABLES

ABBREVIATIONS

ORNL	Oak Ridge National Laboratory
FOV	Field of View
SNS	Spallation Neutron Source

ABSTRACT

The VENUS Neutron Imaging instrument at the Spallation Neutron Source has gone through a multitude of optical design changes since its original conception. The goal of this report is to quantify the performance of the most recent optical design and provide insight into potential improvements to this design as needed to ensure optimal performance of the instrument. The results will come in the form of a refined and well developed simulation that provides as best a representation of the performance of the instrument as reasonably achievable. This simulation will be available in a repository along side relevant simulation output needed to inform any future decisions on the design of the instrument.

1. INTRODUCTION

The VENUS Neutron Imaging Instrument uses a pinhole-style beam configuration utilizing the poisoned and decoupled cryogenic hydrogen moderator at the First Target Station of the Spallation Neutron Source. Given the need to precisely define the optical configuration for this instrument prior to the completion of construction, a simulation describing the beam that arrives at the sample position has been developed. McStas neutron ray-tracing software [1] was used to determine the anticipated beam located at the detector position, under both ideal and practical collimator and scraper geometries. A description of the simulation, additional concepts and other developments used to optimize and quantify the instrument performance will be described herein.

2. VENUS INSTRUMENT DESCRIPTION

The VENUS imaging instrument will be used to understand a range of materials and natural phenomena such as novel alloy development, biological structures, and archaeological discoveries to name a few [2]. The intended mode of the instrument is one that takes data in a transmission configuration with time-of-flight sensitivity to provide wavelength resolution along side the typical radiographic spatial resolution. In its simplest description, the instrument can be represented as a source, an initial aperture, a variable aperture magazine and a detector. The performance of the instrument is determined by the locations and geometries of these apertures, and the neutron beam profile provided by them will impact the design of additional mechanical features downstream. Most notable are two collimators downstream of the variable aperture that will prepare the beam for two distinct Fields of View (FOV); these are 20x20cm and 4x4cm wide configurations. The geometry specifics are presented in Table 1, and are used to understand the anticipated capability and background features, in particular the beam intensity that will not hit the radiography detector.

Table 1. A table describing the basic optical components for the initial VENUS instrument geometry

Component Name	20cm FOV	4cm FOV	Source Distance	Thickness
Source	10cm Wide x 12cm Tall		0.000000 meters	N/A
Fixed Aperture	5.6134 cm Diameter	Same as 20cm FOV	2.549906 meters	4.826 cm
Variable Aperture	Variable Radius	Same as 20cm FOV	4.503293 meters	Variable
Collimator 1	10.5cm Nominal Diameter	5.6cm Nominal Diameter	7.430287 meters	92.339 cm
Collimator 2	12.2cm Nominal Width	4.8cm Nominal Width	12.793193 meters	121.948 cm

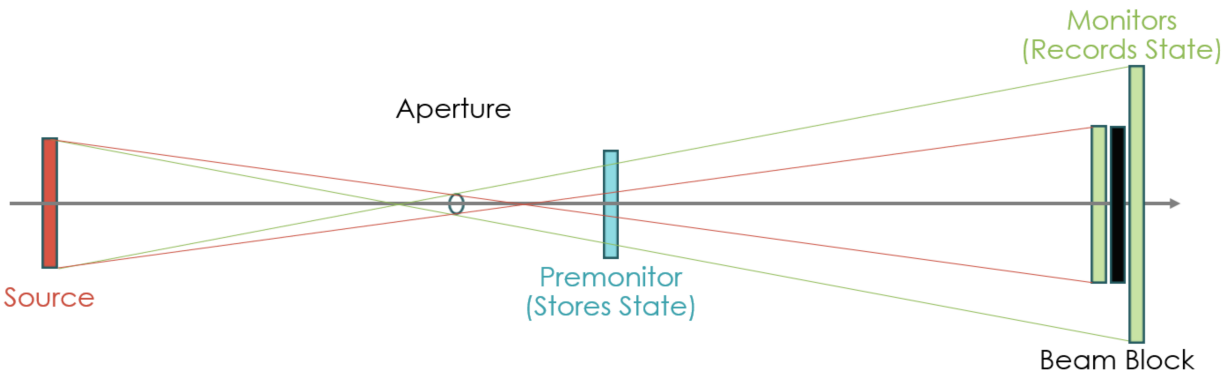

Figure 1. A schematic describing the hit-or-miss flux simulation concept. The Premonitor component (blue) stores the state of the neutron ray at that location, and then the stored state is recorded in one of two files depending on whether or not it ultimately hits the detector (green).

3. SIMPLE SIMULATION RESULTS

The simulation is setup in a way that the beam flux distribution can be observed at the location of each collimator. Furthermore, the beam flux distribution at that location can be measured in such a way to only record that intensity which will ultimately hit or miss the radiography detector. A basic schematic describing this concept can be seen in Figure 1, and its output allows one to precisely identify the outer boundary of the primary beam which will hit the detector. One can see this in Figure 2, where the lowest intensity observed to hit the detector is seen by the outer white contour. The simulation was run with only the most-upstream fixed aperture defining the beam to produce the results seen in that figure (L/D=400). This is the most divergent beam configuration available at VENUS. The importance of determining this boundary is more obvious if one observes the amount of neutron flux that will miss the detector completely. This flux should be rejected as far upstream as possible, as it could only contribute to potential background, and will provide no value at the detector distance. That said, it cannot be understated how important is to not encroach on the primary beam that will be used by the detector. This is the inspiration for utilizing the ideal shapes and is best quantified by the flux distribution of the penumbra intensity that misses the detector.

This shape can be analytically determined by mapping each of the four corners of the detector and projecting an expanding cone towards the aperture location and diameter. This is not too different than the analysis performed by Grünauer in his 2005 dissertation [3], the only real difference being the application from aperture to detector, rather than from the source to the aperture. Furthermore, using CAD software, one can provide the same nominal shape by performing a swept blend from a square with rounded corners of infinitesimally small radius to a circle. This would map eight distinct curves at the detector (four straight, four arcs) to eight equally cut curves at the aperture (eight arcs), and then cross sections taken from spots along this manifold shape. An example of this is seen in Figure 3.

4. MATHEMATICAL DESCRIPTION OF THE IDEAL APERTURE SHAPE

As noted prior, the manifold shape determined by the swept blend and outer limit boundary of the detector "hit" flux distribution can be represented by the shape of a cone. In general, the equation for a cone

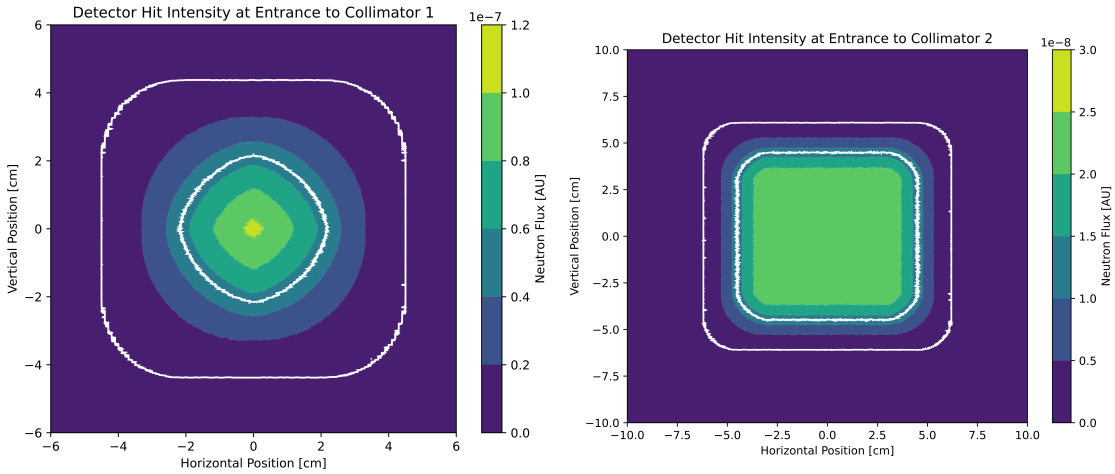

Figure 2. Images describing the flux distribution at the entrance of the collimators.
The "hit" flux at the entrance of Collimator 1 (Left) and Collimator 2 (Right). The lowest recorded values and the half-of-max levels are denoted by the white contours.

in a three-dimensional Cartesian space is

$$(x - \bar{x}(z))^2 + (y - \bar{y}(z))^2 - r(z)^2 = 0$$

Furthermore, the manifold that bounds the range of trajectories permitted between the circular aperture and square detector is represented by an infinite number cones with vertices located on the perimeter of the square. Since the radius, $\bar{x}$ and $\bar{y}$ all depend only on the z position and the shape of the square at the detector position, the centers of the cones between those that connect each corner of the square to the circular aperture lie on a line. Therefore, the shape of a collimator at z between the circular aperture and the square is that of a rounded square.

The defining cone in question for this case is one whose vertex starts at a detector corner and whose base is ultimately represented by the aperture geometry. Using this concept, one concludes that the center location $\vec{r}_{10}(z)$ of a circle along the axis $\vec{r}_{20}(z)$ of that cone can be determined by three points, $\vec{p}_0, \vec{p}_1$ and $\vec{p}_2$

$$\vec{p}_0 = (x_0, y_0, 0), \qquad \vec{p}_1 = (0, 0, L), \qquad \vec{p}_2 = (R, 0, L)$$

$$\vec{r}_{10} = \vec{p}_0 + z\frac{(\vec{p}_1 - \vec{p}_0)}{(\vec{p}_1 - \vec{p}_0)\cdot\hat{z}} = (x_c(z), y_c(z), z)$$

$$\vec{r}_{20} = \vec{p}_0 + z\frac{(\vec{p}_2 - \vec{p}_0)}{(\vec{p}_2 - \vec{p}_0)\cdot\hat{z}} = (x_0 + z\frac{R}{L}, y_0 - z\frac{y_0}{L}, z)$$

$$\vec{r}_c(z) = (x_0(1 - z/L), y_0(1 - z/L), z) \qquad R_c(z) = |\vec{r}_{20}(z) - \vec{r}_c(z)| = z\frac{R}{L}$$

Here, R is the radius of the aperture, x_0 and y_0 are the coordinates at corner of the detector, and L is the distance between the detector face and aperture. The corner coordinates are used here as they define the extreme points of the geometry, but one could use any location on the detector to understand what range of the trajectory space will be transmitted by the aperture to that location. The approximate result is a set of defined cones that directly define the specific geometry needed to allow the collimators to be directly suited to the optical design.

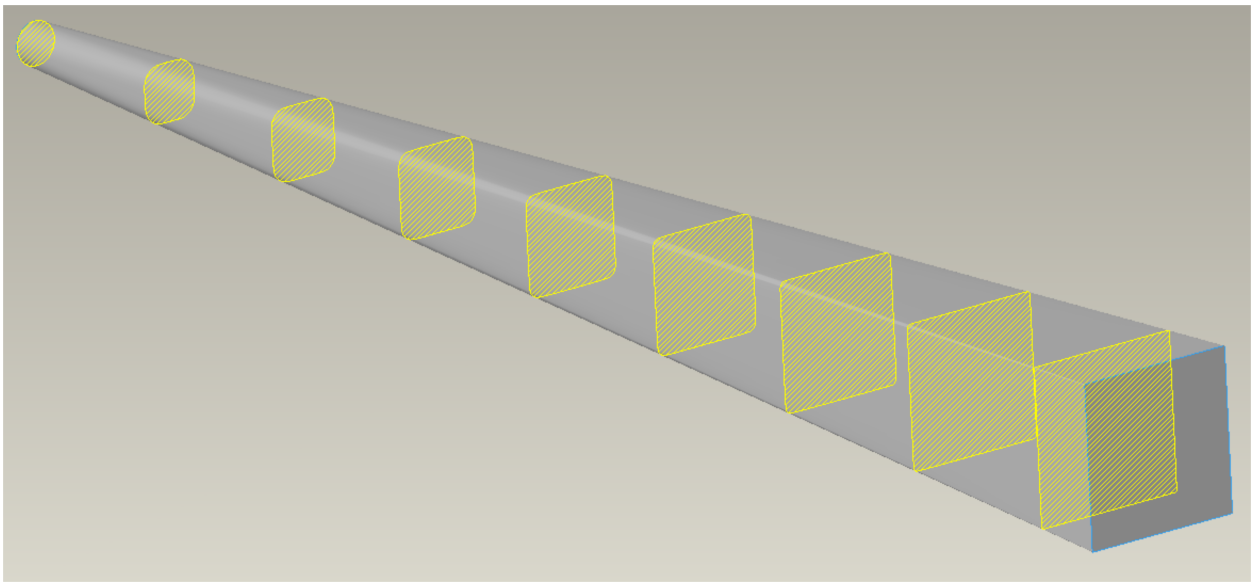

Figure 3. A swept blend in Creo CAD modeling software. One can see the slow change in shape from circular aperture to a square detector along the nominal beam trajectory.

For the each FOV configuration, we use the four points that define the detector corners, the radius on the downstream side of the L/D=400 aperture configuration, the distance from that point to the detector, and a set of locations along the beam to specify the shape. For these shapes, we use the downstream plane of the optical component for those locations, as this will provide the least encroachment into the primary beam while at the same avoiding the need to taper the cut through the defining aperture.

One can see the results of these calculations in Tables 2 and 3. A plot showing these shapes for both FOV configurations at each aperture location along z can be seen in Figure 4

4.1 PRACTICAL COLLIMATOR APERTURE SHAPES

If one where to only permit circular and square apertures to be used the best route would be to use only square apertures for the 20cm FOV configuration. The 4cm FOV configuration should use circular apertures

Table 2. A table describing the specific geometry that should be implemented to minimize penumbra beam intensity near the detector for 20cm FOV. The results are based on as-designed values for the downstream plane positions of the boron-nitride collimator apertures. Center coordinates for the position are the same for all corners, with the need to negate depending on which quadrant the circle is located.

Component Name	z Position [meters]	Corner Radius [cm]	Quadrant I Center Coordinates [cm]
Collimator 1 US	7.476287	2.1955	2.1776, 2.1776
Collimator 1 DS	8.399678	2.0798	2.5897, 2.5897
Collimator 2 US	12.839192	1.5236	4.5715, 4.5715
Collimator 2 DS	14.058671	1.3708	5.1159, 5.1159
Scraper 1	16.069994	1.1188	6.0137, 6.0137
Scraper 2	16.569994	1.0562	6.2369, 6.2369
Scraper 3	17.069994	0.9935	6.4601, 6.4601

Table 3. A table describing the specific geometry that should be implemented to minimize penumbra beam intensity near the detector for 4cm FOV. The results are based on as-designed values for the downstream plane positions of the boron-nitride collimator apertures. Center coordinates for the position are the same for all corners, with the need to negate depending on which quadrant the circle is located.

Component Name	z Position [meters]	Corner Radius [cm]	Quadrant I Center Coordinates [cm]
Collimator 1 US	7.476287	2.1955	0.4355, 0.4355
Collimator 1 DS	8.399678	2.0798	0.5179, 0.5179
Collimator 2 US	12.839192	1.5236	0.9143, 0.9143
Collimator 2 DS	14.058671	1.3708	1.0232, 1.0232
Scraper 1	16.069994	1.1188	1.2027, 1.2027
Scraper 2	16.569994	1.0562	1.2474, 1.2474
Scraper 3	17.069994	0.9935	1.2920, 1.2920

for the upstream collimator and square apertures for the down stream collimators. The ideal square width, W, can be found by

$$W = 2 \times (R + CC)$$

where R is the radius and CC is the center coordinates as specified in the third and fourth columns of the Table 2 or 3. The ideal circle radii, B, can be found by

$$B = \sqrt{2}CC + R$$

using the same nomenclature as from the ideal square calculation.

5. SIMULATION RESULTS

Using the developed VENUS McStas simulation [4], we are able to determine how much of an impact to the penumbra intensity each aperture can have. This determination is made in three ways, the first being the improvement of penumbra intensity around the detector as a result of the entire compliment of apertures. The second is a comparison by the relative increase in area of either a square or circular aperture as compared to the calculated ideal shape, and the third uses the same nominal area comparison but weighted by the penumbra intensity that would be permitted by those coinciding areas. This weighting is provided by the Premonitor "miss" flux distribution.

5.1 PENUMBRA INTENSITY DISTRIBUTION

The "penumbra" as defined in this context is strictly the beam intensity from the source/aperture/collimator configuration that will miss the detector. The direct impact that the collimators have on the penumbra can be seen in Figures 5 and 6. As these results are strictly ray tracing in nature and do not represent any background contributions that may come about due to scattering or gamma production, they do not provide a good comparison of between the Practical and Ideal collimating geometries. Nonetheless, they are still do provide a good estimate of the penumbral beam intensity arriving at the same location in addition to the beam in the FOV.

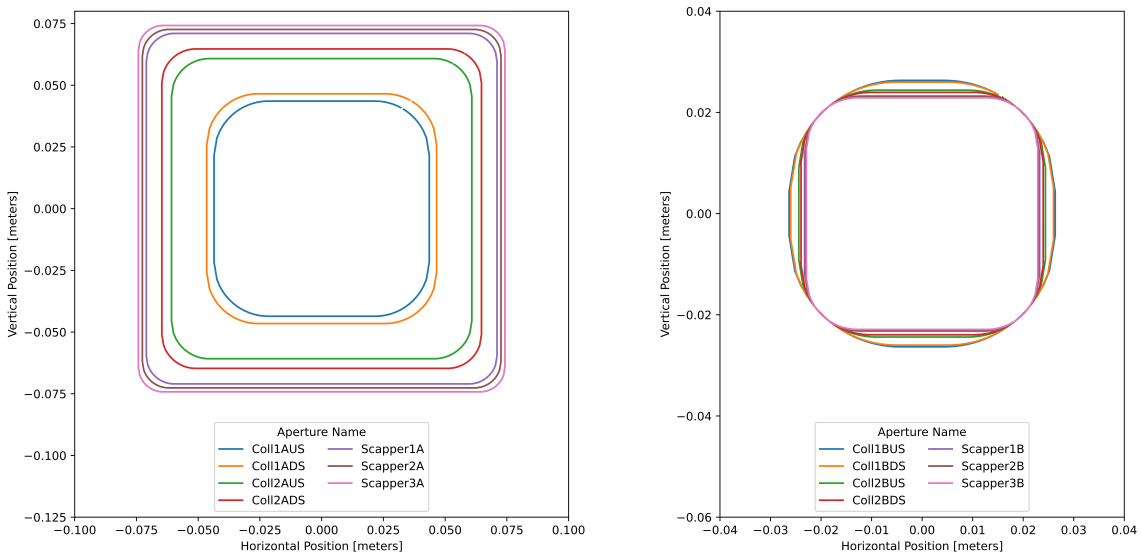

Figure 4. Calculated ideal shapes for downstream sides of each aperture. The 20cm FOV configuration is shown on the Left, and the 4cm FOV configuration is shown on the right.

5.2 AREA COMPARISON OF DIFFERENT APERTURE GEOMETRIES

Due to the potential effects of background, it would be prudent to emphasize the *potential* impact a shape could have assuming that it is the only aperture affecting the detector. This is important as any beam change that is not done by the aperture at its location would only burden the apertures downstream, or potentially make it to the detector position and become the source of a local background feature. A comparison of the areas amongst the different shapes at each location can be seen in Table 4. Furthermore, the simulations performed prior provide one with a penumbra beam intensity distribution at the location of each aperture. Taking the additional area determined in Table 4 and weighting it with the simulated position of the flux distribution at the location of aperture along the beam will provide and even better representation of how much penumbral beam intensity would be passed by the aperture. A comparison of the areas amongst the

Table 4. A table describing difference in relative area between the practical and ideal aperture shapes. These can be used as a first order comparison to understand the potential impact an aperture will have on the background at the detector position.

Aperture\Shape	FOV 20cm		FOV 4cm	
	Square [%]	Circle [%]	Square [%]	Circle [%]
Collimator 1 US (Area% more than Ideal)	5.8	20.6	17.7	5.4
Collimator 1 DS (Area% more than Ideal)	4.5	23.9	16	6.7
Collimator 2 US (Area% more than Ideal)	1.4	36.6	9.2	14.3
Collimator 2 DS (Area% more than Ideal)	0.98	39.5	7.6	16.9
Scraper 1 (Area% more than Ideal)	0.55	43.5	NA	NA
Scraper 2 (Area% more than Ideal)	0.47	44.5	NA	NA
Scraper 3 (Area% more than Ideal)	0.4	45.4	NA	NA

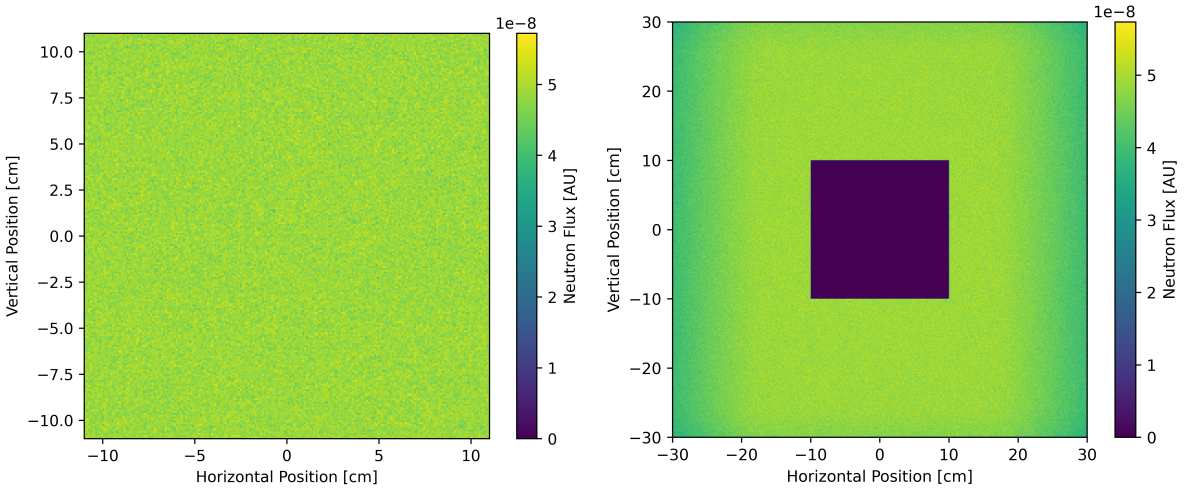

Figure 5. Penumbra Intensity with no Collimation. The simulated distribution on the detector is shown on the left, and the penumbra intensity that will miss the detector is on the right.

different shapes weighted with the simulated penumbral beam intensity can be seen in Table 5.

6. CONCLUSION AND ACKNOWLEDGEMENTS

In general, one should select an aperture set that would permit the least amount of penumbra intensity through as close to the front as possible. This suggests that using the ideal shapes would be the best option based on the analysis provided in Section 5.2. The methods used to define those shapes are in Section 4. and precise definitions for the supplied collimator locations can be seen in Tables 2 and 3. The authors would like to acknowledge Franz Gallmeier and Irina Popova for their contribution to discussions and initial review.

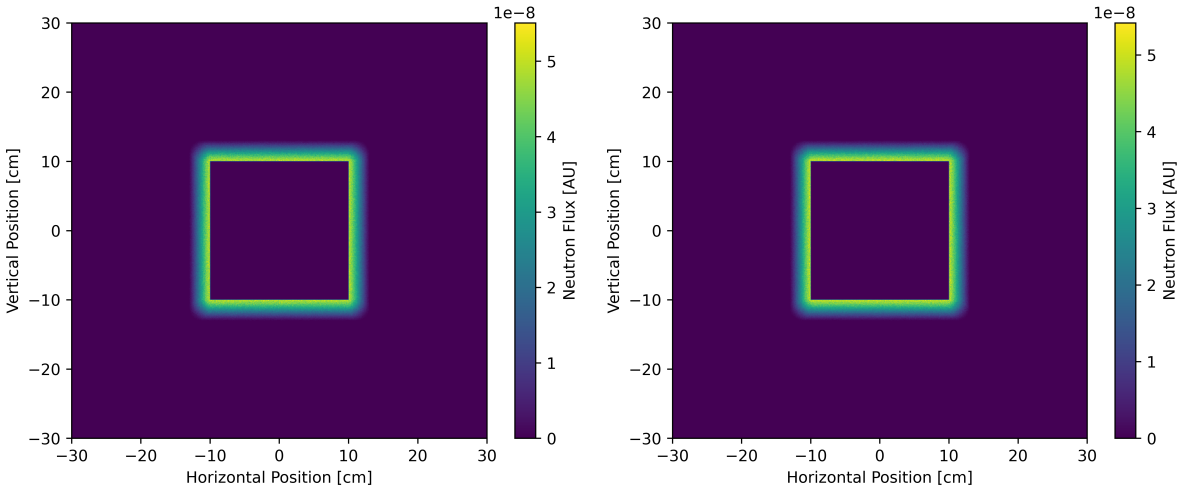

Figure 6. Penumbra Intensity with Collimation. A comparison between the practical collimator geometry and the ideal collimator geometry . The reduction in total intensity in the penumbra region for both configurations is 98.5%. The difference between the two is negated by the dominance of the square scrapers used in both configurations, and neither disrupt the beam intensity distribution on the detector itself.

Table 5. A table describing difference in relative weighted area between the practical and ideal aperture shapes. These can be used as a better comparison to understand the potential impact an aperture will have on the background at the detector position.

Aperture\Shape	FOV 20cm		FOV 4cm	
	Square [%]	Circle [%]	Square [%]	Circle [%]
Collimator 1 US (Area% more than Ideal)	7.1	27.4	18.1	4.8
Collimator 1 DS (Area% more than Ideal)	6.4	34.4	13.9	8.2
Collimator 2 US (Area% more than Ideal)	2.8	89.9	11.4	16.4
Collimator 2 DS (Area% more than Ideal)	2.3	110.8	7.2	24.2
Scraper 1 (Area% more than Ideal)	2.6	143.8	NA	NA
Scraper 2 (Area% more than Ideal)	1.7	172.4	NA	NA
Scraper 3 (Area% more than Ideal)	2	179.2	NA	NA

References

[1] Peter Kjaer Willendrup and Kim Lefmann. McStas (ii): An overview of components, their use, and advice for user contributions. *Journal of Neutron Research*, 23(1):7–27, April 2021.

[2] Hassina Bilheux, Ken Herwig, Scott Keener, and Larry Davis. Overview of the Conceptual Design of the Future VENUS Neutron Imaging Beam Line at the Spallation Neutron Source. *Physics Procedia*, 69:55–59, 2015.

[3] Florian Grünauer. *Design, optimization, and implementation of the new neutron radiography facility at FRM-II*. PhD thesis, TECHNISCHE UNIVERSITÄT MÜNCHEN, September 2005.

[4] Matthew J. Frost and Christoph U. Wildgruber. VENUS, November 2022. https://code.ornl.gov/sns-neutronics/mcstas-wg/venus.

APPENDIX

A DEFINITION OF A TILTED RIGHT CIRCULAR CONE

A right circular cone in the $\hat{x} - \hat{y}$ plane is described by the general equation:

$$(x - \bar{x})^2 + (y - \bar{y})^2 - r(z)^2 = 0, \tag{1}$$

where $\bar{x}$ and $\bar{y}$ are the center of the circular base and the radius is a function of z.

The radius of the circular cross section of the cone parallel to the first aperture is given by

$$r(z) = \frac{z - z_1}{z_0 - z_1} r_0, \tag{2}$$

The location of the center of the circular cross section of the cone parallel to the first aperture is given by

$$\bar{x}(z) = x_0 + \frac{x_1 - x_0}{z_1 - z_0}(z - z_0) \tag{3}$$

$$\bar{y}(z) = y_0 + \frac{y_1 - y_0}{z_1 - z_0}(z - z_0) \tag{4}$$

$$z = z, \tag{5}$$

where the center of the circular aperture is at (x_1, y_1, z_1), with radius r_0, and the apex of the cone is at (x_0, y_0, z_0).

The expansion of the equation of the cone

$$(x - \bar{x}(z))^2 + (y - \bar{y}(z))^2 - r(z)^2 = 0 \tag{6}$$

is a quadric of the form

$$Ax^2 + By^2 + Cz^2 + Dxy + Eyz + Fzx + Gx + Hy + Jz + K = 0, \tag{7}$$

and these coefficients are given by

$$A = 1 \tag{8}$$

$$B = 1 \tag{9}$$

$$C = \frac{\Delta_x^2 + \Delta_y^2 - r^2}{\Delta_z^2} \tag{10}$$

$$D = 0 \tag{11}$$

$$E = \frac{2y_1 - 2y_0}{\Delta_z} \tag{12}$$

$$F = \frac{2x_1 - 2x_0}{\Delta_z} \tag{13}$$

$$G = \frac{2x_0 z_1 - 2x_1 z_1}{\Delta_z} - 2x_1 \tag{14}$$

$$H = \frac{2y_0 z_1 - 2y_1 z_1}{\Delta_z} - 2y_1 \tag{15}$$

$$J = \frac{2r^2 z_0 - 2z_1(\Delta_x^2 + \Delta_y^2)}{\Delta_z^2} + \frac{2y_1 y_0 - 2y_1^2 + 2x_1 x_0 - 2x_1^2}{\Delta_z} \tag{16}$$

$$K = \frac{z_1^2(\Delta_x^2 + \Delta_y^2) - r^2 z_1^2}{\Delta_z^2} + \frac{2z_1(y_1^2 - y_1 y_f + x_1^2 - x_1 x_0)}{\Delta_z} + y_1^2 + x_1^2, \tag{17}$$

where

$$\Delta_x = x_0 - x_1 \tag{18}$$
$$\Delta_y = y_0 - y_1 \tag{19}$$
$$\Delta_z = z_0 - z_1. \tag{20}$$

B CONNECTING A CIRCLE TO A SQUARE

The bounding surface around the allowable rays that pass through a circle at (x_1, y_1, z_1) and a square of dimension s with corners at

$$s1 = \left(+\frac{s}{2}, +\frac{s}{2}, z_0\right) \tag{21}$$
$$s2 = \left(-\frac{s}{2}, +\frac{s}{2}, z_0\right) \tag{22}$$
$$s3 = \left(-\frac{s}{2}, -\frac{s}{2}, z_0\right) \tag{23}$$
$$s4 = \left(+\frac{s}{2}, -\frac{s}{2}, z_0\right), \tag{24}$$

is determined by projecting an infinite number of tilted cones from points on the perimeter of the square to the circle. The radius of these cones depends only on the z position and the radius of the circular aperture. Additionally, the $\bar{x}$ and $\bar{y}$ of all cones with apexes along a single edge of the square are co-linear at a specified z position. Therefore, the shape of an aperture at z between the circle and the square is that of a rounded square, which is a circle of radius

$$r(z) = \frac{z - z_0}{z_1 - z_0} r_1 \tag{25}$$

that is split into four identical pieces, separated, and connected by straight lines of length

$$w(z) = \frac{z - z_1}{z_0 - z_1} s. \tag{26}$$

At the limits, we have

$$r(z_1) = r_1 \tag{27}$$
$$r(z_0) = 0 \tag{28}$$
$$w(z_1) = 0 \tag{29}$$
$$w(z_0) = s, \tag{30}$$

and each varies linearly with z.